Interactive life-history traits predict sensitivity of plants and animals to temporal autocorrelation

Maria Paniw[1,2*], Arpat Ozgul[1], Roberto Salguero-Gómez[3,4,5,6]

[1] Department of Evolutionary Biology and Environmental Studies, University of Zurich, Zurich 8057, Switzerland

[2] Department of Biology, University of Cadiz, Puerto Real 11510, Spain

[3] Department of Zoology, Oxford University, New Radcliffe House, Radcliffe Observatory Quarter, Woodstock Rd, Oxford OX2 6GG, UK

[4] Department of Animal & Plant Sciences, University of Sheffield, Alfred Denny Building, Western Bank, Sheffield, S10 2TN. UK.

[5] Centre for Biodiversity and Conservation Science, University of Queensland, St Lucia 4071 QLD, Australia

[6] Evolutionary Demography Laboratory, Max Plank Institute for Demographic Research, Rostock 18057, Germany

*Correspondence: maria.paniw@ieu.uzh.ch

Table of contents

The data and *R* scripts used for simulations and described in the following can be found on:

https://github.com/MariaPaniw/patterns_temporal_autocorrelation

See also Dryad doi:10.5061/dryad.d851q for the archived data supporting the results.

Appendix S1 Database, data selection, and vital rates

We used matrix population models (MPMs) from the COMADRE Animal Matrix Database (version 2.0.1; Salguero-Gómez *et al*. 2016a) and the COMPADRE Plant Matrix Database (version 4.0.1; Salguero-Gómez *et al*. 2015) using the following selection criteria:

- MPMs that are primitive, irreducible and non-negative so that we could reliably calculate important demographic quantities such as the population growth rate, λ, or damping ratio
- MPMs reporting genet (whole genetically-identical individual) dynamics. We excluded clonal species examined at the ramet level to facilitate analysis and interpretation of results (*i.e.*, not to mix genet and ramet dynamics), and because in many cases clonal species are only examined at the genet level when using MPMs (R. Salguero-Gómez, unpubl. data).
- MPMs for which vital rates of distinct demographic nature (e.g. survival, sexual reproduction) could be reliably retrieved - *i.e.*, non-zero fecundity and transition matrices were available separately, so that various demographic processes within a single matrix element, when occurring, were clearly differentiated (Salguero-Gómez *et al*. 2015).
- MPMs reporting population dynamics under unmanipulated conditions only (e.g. no experimental sites or laboratory conditions) so as to exploring patterns of autocorrelation under natural settings.
- The phylogeny of the species is resolved (see Appendix S2), as we required phylogenetic information for our analyses because inter-specific relationships among life-history traits may be affected by the phylogenetic relatedness among species.

After applying these criteria, we obtained 454 MPMs corresponding to multiple years within populations, and when available, multiple study sites, for each of the 327 plant/algae and 126 animal populations. Most matrices represented a unique species (449 in total). If the population dynamics of a given species where reported for different sites by different publications, we kept all these species' specific MPMs from multiple studies only if their geographic provenance resulted in them being in distinct habitat types and populations showed markedly different vital rates. We consulted the original publications MPMs were obtained from to decide whether to keep or discard a population. If different publications reported on the same population, we chose the publication with the greatest temporal and spatial MPM replicates to better represent the species' population dynamics. For studies providing vital-rate data from several sites or study periods, the MPMs used in this study corresponded to the element-by-element arithmetic mean matrices across all studied sites and periods within a population. Information on all the 454 populations can be found in *phyloSpecies.csv*.

For each of the 454 populations, we retrieved information on the habitat type (*i.e.*, ecoregion) populations were found in, in order to explore differences in species' sensitivity to temporal autocorrelation among habitat types. More information on how ecoregions are derived in COMADRE and COMPADRE can be found in Salguero-Gómez *et al*. (2015, 2016a). To increase the statistical power of analyses, we reduced the 39 ecoregions found in our data selection down to five. The five resulting major habitats were: *Temperate*, *Tropical & subtropical*, *Arid, alpine & arctic*, and *Aquatic*, following Salguero-Gómez *et al*. (2016b).

In order to perturb vital rates during simulations, we extracted all vital rates per MPM as shown in `getVitalRates.R`. Briefly, we obtained stage/age-specific reproduction (f) from the fecundity (F) MPM and survival (s) and progression (g) and retrogression (r) from the

survival-dependent transition (U) MPM. All survival and reproduction vital rates were corrected for the periodicity of transitions under which the original MPMs were parameterized – *i.e.*, inverse of number of years elapsed since consecutive measures of vital rates – as shown in `getVitalRates.R` (lines 162 & 216). This allowed for life-history comparisons among populations on the same temporal (annual) scale (Appendix S2). We obtained information on the periodicity of MPMs from the COMPADRE and COMADRE databases.

To facilitate comparison of differences in simulated demographic processes among various life history strategies (Appendix S3), we also assigned each vital rate to one the following groups as shown in `getVitalRates.R` (lines 227-261; Salguero-Gómez & Plotkin 2010):

- Propagule (P): dormant life stages such as seed banks or diapause.
- Pre-reproductive (PR): pre-reproductive individuals (with above-ground mass, for plants).
- Reproductive (R): individuals that produce offspring (P or PR, or R).
- Non-reproductive (NR): adult individuals that were reproductive before but not currently.

Appendix S2 Phylogenies and PCA analyses

To implement the phylogenetic comparisons in our study, we built a super-tree constituted by three species-level phylogenies for animals (*AnimalPhylo.nexus*), plants (*PlantPhylo.tre*), and algae (*AlgaePhylo.tre*). We used the phylogenetic information from the Open Tree of Life (OTL; Hinchliff *et al*. 2015; https://tree.opentreeoflife.org). OTL is an open-access database of taxonomic and phylogenetic information integrated into a single tree of life. Using the *rotl* package (Michonneau *et al*. 2016) we downloaded algae, plant and animal trees from the list of

species in our data, after these had been taxonomically updated using the R library *taxize* (Chamberlain & Szocs 2013). We then created a supertree using the function *bind.tree* in the *phytools* package (Revell 2012), assembling first plants and algae trees, and next the animal tree. Branch length was computed using the *compute.brlen* in the R package *ape* (Paradis *et al*. 2004). Polytomies were collapsed using the function *multi2di* from the former package, which transforms polytomies into a series of random dichotomies with one or several zero-length branches. For those species where more than population was examined (n = 5 species), we also coerced branches at their species-level tips to include multiple populations. The *R* script `phyloPCA.R` details how to construct a super tree out of the three phylogenies and link it to the species' demographic data (described in Appendix S1).

We used a phylogenetically informed principal-component analysis (PCA) approach to quantify patterns in the variation of life-history traits among taxa that then would serve as predictors of species' population responses to variation in autocorrelation in environmental variation (Appendix S3). We used key life-history traits (Table S2.1) that are known to explain most of the variation in demographic performance in deterministic environments for plants (Salguero-Gómez *et al*. 2016b) and animals (Salguero-Gómez unpubl. data). As we aimed to make a general comparison of life histories across plants and animals, we did not include progression and retrogression, which, despite explaining important differences in plant life histories (Salguero-Gómez *et al*. 2016b), is not measurable in most animal MPMs, which are age-based (Salguero-Gómez *et al*. 2016a). We also excluded Keyfitz' entropy (Keyfitz 1977; Salguero-Gómez *et al*. 2016b) and mature life expectancy, because calculation of these measures were either insolvable (Keyfitz' entropy) or produced negative values (mature life expectancy) for > 10 % of species. Including both measures into the PCA for a subset of species did not

significantly improve the variation explained by the two PCA axes (not shown), and we concluded that including five life-history traits sufficed to provide a good spread of data on the PCA landscape. A detailed description of how traits are calculated can be found in Caswell (2001, ch. 5) and Salguero-Gómez *et al*. (2016b). The *R* script `phyloPCA.R` implements the derivation of the five life-history traits used in this study.

Table S2.1 Description of the life-history traits used to explore the variation in life-history strategies in the studied 415 plant/algae and animal populations. λ – population growth rate (dominant eigenvalues of species' matrix population model); φ – fecundities (for collapsed matrices, values correspond to φ_{PR}, φ_{JR}, and φ_{RR}); $l_x m_x$ – age-specific (x) survival and mortality.

Trait	Description	Formulae
Generation time (T)	Average time between two consecutive generations	$T = \frac{\log(R_o)}{\log(\lambda)}$
Age at sexual maturity (L_α)	Time (years) at which an average individual in a population becomes reproductive	Ch. 5.3.3 in Caswell (2001)
Annual sexual reproduction (ϕ)	Total number of recruits from sexual reproduction in the life-cycle of a species (Fig. S1.1) in a given year	$\phi = \sum_1^3 \varphi$
Degree of iteroparity (S)	Spread of reproduction throughout the lifespan of an average individual in the population (Demetrius' entropy, S). Low S – semelparous reproduction; high S – iteroparous reproduction	$S = -e^{-\log(\lambda)} l_x m_x \log(e^{-\log(\lambda)} l_x m_x)$
Net reproductive rate (R_o)	Mean number of recruits produced by an average individual during its mean life expectancy, as determined by its age-specific survival (l_x) and fertility (m_x) schedules	$R_o = \int_0^\infty l_x m_x dx$

Our approach aimed at describing different life-history strategies from the 454 populations, while accounting for their phylogenetic relatedness. PCA reduces the dimensionality of data by quantifying the preponderant axes that are necessary to explain a given percentage of variation of the data. Prior to performing the PCA, we used a log transformation on the trait values to ensure a normal distribution of values. After transforming the data, we rescaled them to $\mu = 0$ and SD = 1. We then implemented the phylogenetically informed PCA using the

phyl.pca function in the *R* library *phytools* (Revell 2012). This package uses maximum likelihood to estimate Pagel's λ while conducting the PCA. Pagel's λ (not to be confused with population growth rate λ) is scaling parameter for the phylogenetic correlation between species that ranges from 0, *i.e.*, no role of phylogeny in determining trait variation, to 1, *i.e.*, trait variation fully explained by phylogeny (Freckleton *et al*. 2002; Appendix S2). The quantification of Pagel's λ assumes that traits evolve via a process of Brownian motion.

After implementing the PCA, we used the Kaiser criterion (Legendre & Legendre 2012) to explore how many axes sufficiently explain the variation observed in the data. This criterion is based on keeping only principal component axes with associated eigenvalues > 1. We then performed a variance maximizing rotation of the significant PCA axes as demonstrated in `phyloPCA.R`. Table S2.2 below shows the full results obtained from the PCA analysis.

Table S2.2 Loadings of life-history traits (rows; Table S2.1) on the principle component axes. The first two axes, which together explain 66% of the variation in the data and have associated eigenvalues > 1 (in bold), are varimax-corrected. Redder colors identify more positive loadings while bluer colors identify more negative loadings. % var. – percent variation explained by each principle component axis; Cumulative var. – cumulative variance explained.

Life-history trait	PCA 1	PCA 2	PCA 3	PCA 4	PCA 5
T	0.88	-0.12	-0.25	-0.20	0.32
L_α	0.91	0.11	0.00	0.22	-0.34
ϕ	-0.17	0.71	-0.51	0.43	0.09
S	-0.04	0.79	-0.14	-0.58	-0.13
R_o	0.21	0.71	0.63	0.14	0.16
Eigenvalue	**1.68**	**1.66**	0.87	0.80	0.52
% Var.	33.5	33.1	15.2	12.7	0.05
Cumulative var.	33.5	66.7	81.8	94.6	100.0

To test how extreme life-history traits affected our results, we also performed the PCA after excluding outliers in each log-transformed life-history trait. Here we defined outliers as those values outside the 2.5th-97.5th percentile range. However, our results did not change qualitatively after removing outliers (not shown). We also tested the robustness of our results by repeating PCA analyses for plants/algae and animals separately (Fig. S2.1).

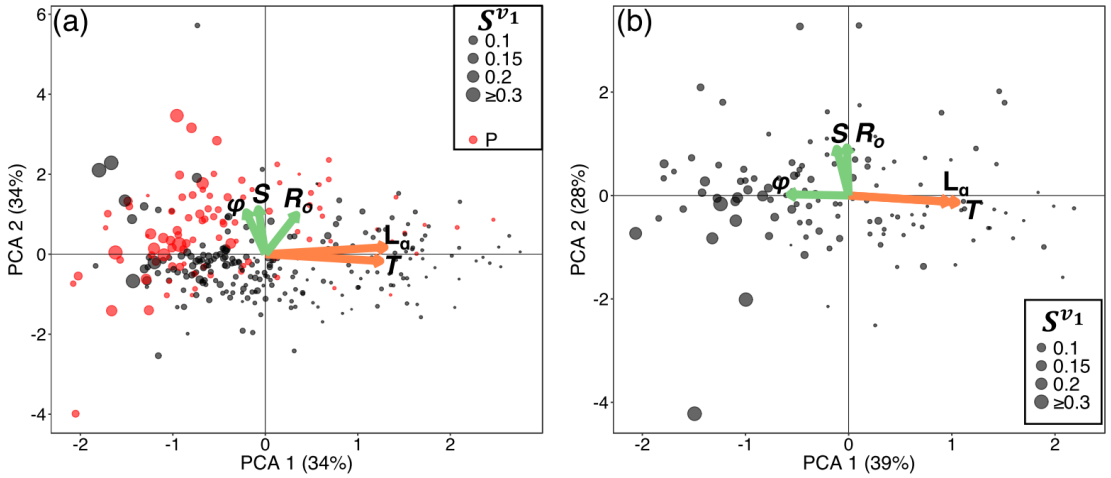

Figure S2.1 First two components of a phylogenetically-informed PCA performed on life-history traits (Table S2.1; arrows) obtained from MPMs of 454 populations. PCA were performed for 327 plants/algae (a) and 126 animals (b) separately (shown together in Fig. 2). Arrow lengths are proportional to the loadings of each trait onto PCA 1 and 2. Point sizes are proportional to average absolute sensitivity of the stochastic population growth rate to temporal autocorrelation, S^{v_1}, across vital rates (for simulations at CV = 0.5 and f = 0.65 are shown here; see Appendix S3). Pagel's λ = 0.48 (± 0.11 S.D.) for plants/algae (a) and Pagel's λ = 0.63 (± 0.14 S.D.) for animals (b). Red points correspond to populations with propagule (P) stages.

Phylogenetically informed PCA performed on plant/algae and animal populations separately yielded similar characterizations of variation in life-history strategies, the fast-slow (PCA 1) and reproductive-strategies (PCA 2) continua, but also showed some differences. The major difference between plants/algae and animals was that the total reproduction (φ) for the latter was strongly associated with the fast-slow instead of the reproductive-strategies continuum and was highest for fast life histories (Fig. S2.1). This means that unlike plants, where life

histories are more varied, short-lived animal species also produce many offspring, which can be explained by strong survival-reproduction trade-offs present in animals (Cohen 2004) or perhaps sampling differences in the status quo of animal vs. plants demography (Salguero-Gómez *et al*. 2016b). At the same time, sensitivities of the stochastic population growth rate, log λ_s, to temporal autocorrelation, S^{v_1} (Appendix S3) were highest for fast life histories with high annual reproduction (ϕ) and across a range of net reproductive rates (R_o) and degrees of iteroparity (S) – for both plant/algae and animal populations considered separately (Fig. S2.1). Detailed comparative analyses among plants and animals were beyond the scope of this work.

One key aspect of the PCA analyses was that the resulting main axes (PCA 1 and PCA 2) are evolutionarily independent, *i.e.*, the phylogenetic correlation between scores on each axis = 0 (Revell 2009). However, variation in S^{v_1}may have a phylogenetic component not explained by the PCA axes. To test whether the PCA absorbed most phylogenetic variation in S^{v_1}, we modeled S^{v_1} (summed over all vital rates as described in Appendix S3) as a function of PCA 1 and PCA 2 using phylogenetic generalized least square models (*pGLS*; Orme *et al*. 2013; see lines 570-701 in R script `phyloPCA.R`). These preliminary analyses showed that the effect of phylogeny on summed S^{v_1}, after accounting for life history, were negligible (*i.e.*, the best performing *pGLS* model was obtained with a low Pagel's λ = 0.15). Figure S2.2 also demonstrates that predictions of *pGLS* models do not differ significantly after increasing Pagel's λ in the models (thereby assuming a stronger effect of phylogeny). Therefore, as the the PCA sufficiently corrected for the non-independence among life histories, in terms of phylogeny, we did not include phylogeny when modeling S^{v_1}using GAMs (Appendix S3).

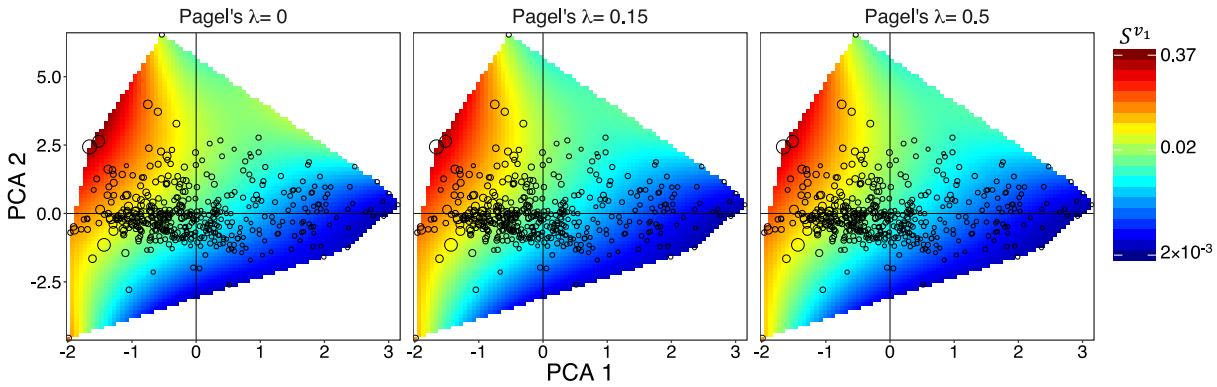

Figure S2.2 Raster plots show predictions of S^{v_1} summed for all vital rates (using simulations at CV = 0.5 and f = 0.65; see Appendix S3) across the two PCA axes depicting different life-history strategies. Model predictions were obtained from phylogenetic generalized least square models assuming various strength of the phylogenetic correlation among species (Pagel's λ). Points are proportional to raw S^{v_1} for obtained from simulations.

Appendix S3 Simulations of temporal autocorrelation

Mean vital rates from matrix population models (MPMs) obtained in Appendix S1 were perturbed using the steps in the *R* script `simLambdaTAC.R`. Using the mean vital rates, we determined new averages for good and bad environmental conditions by sampling randomly from truncated gamma and beta distributions for stage/age-specific fecundity (*f* in script) and survival (*s*)/progression (*g*)/retrogression (*r*), respectively. More concretely, for a gamma-distributed vital rate *x*, the mean value in a good environment (μ_{gx}) was obtained from the average of *n* = 10,000 draws of the gamma distribution truncated above the mean of the vital rate (μ_{ox}) obtained from COMADRE and COMPADRE (Appendix S1):

$$\mu_{gx} = \frac{\sum_1^n Gamma(x|\mu_{ox} < X;\ \alpha, \beta)}{n}$$

with $\alpha = \frac{\mu_{ox}^2}{(CV \times \mu_{ox})^2}$ and $\beta = \frac{(CV \times \mu_{ox})^2}{\mu_{ox}}$, where CV took values of 0.2, 0.5, or 0.8.

Similarly, for a beta-disturbed vital rate *y*, μ_{gy} was obtained as:

$$\mu_{gy} = \frac{\sum_1^n Be(x|\mu_{oy} < X < 1;\ \alpha, \beta)}{n}$$

with $\alpha = \mu_{oy}\left(\frac{\mu_{oy}(1-\mu_{oy})-1}{(CV\times CV_{maxy}\times\mu_{oy})^2}\right)$ and $\beta = (1-\mu_{oy})\left(\frac{\mu_{oy}(1-\mu_{oy})-1}{(CV\times CV_{maxy}\times\mu_{oy})^2}\right)$.

Here, $CV_{max} = \frac{\sqrt{\mu_{oy}(1-\mu_{oy})}}{\mu_{oy}}$ and defined the maximum coefficient of variation given the mean.

The mean vital rate for the bad environment (μ_b) was obtained analogously, but setting the upper, not the lower, bound of X to μ_{ox} or μ_{oy} (`simLambdaTAC.R`). We used the average of the randomly generated values instead of the full random sample because we wanted to separate between (given by μ_g and μ_b) and within environmental-state variance. To simulate within environmental-state variance for each perturbed vital rate, we sampled 100 values from a gamma (when perturbing fecundities) or beta (survival/progression/retrogression) distribution with a CV = 0.01 and $\mu = \mu_g$ or $\mu = \mu_b$ representing, respectively, good and bad environmental conditions. Thus, for each environmental state, we constructed 100 MPMs that were randomly sampled for a given environmental condition at iteration *t* during simulations of the stochastic population growth rate, log λ_s. We kept the coefficient of variation small because the main focus of our investigations was not on the within environmental state variance, and we therefore intended to keep its influence low.

To explore how much constraining the variation in binomial vital rates by CV_{max} affected our simulations of vital-rate differences among environmental states, we also assigned vital rates to good and bad environmental states without modeling vital-rate distributions. That is, we composed MPMs for good and bad environmental states by perturbing a vital rate *x* away from its average value (μ_{ox}) based on the CV simulated without controlling for CV_{max}. Regardless of whether we perturbed fecundities or survival/progression/retrogression, the new average value of

the good environmental state was then: $\mu_{gx} = \mu_{ox} + (\mu_{ox} \times CV)$. Equivalently, for the bad environmental state: $\mu_{bx} = \mu_{ox} - (\mu_{ox} \times CV)$. No within-state variance was modeled. The values of μ_{gx} and μ_{bx} were only constrained to fall in the range [0,1] for survival and growth rates and $[0, +\infty]$ for fecundities. Fig. S3.1 below shows the distribution of vital rates among good (upper error bar) and bad environmental states (lower bar) under the various CV assumptions for a small subset of species at simulated CV = 0.5 (for all species at CV = 0.5, see *CV_survival_transitions.pdf* and *CV_reproduction.pdf*). It is notable that omitting CV_{max} resulted in a larger variation of binomial vital rates (grey error bars; Fig. S3.1a) with high average values than ones with small averages. The opposite was true when CV_{max} was modeled (red error bars; Fig. S3.1a). When vital-rate distributions were imposed, including CV_{max}, approximated well observed variation in vital rates (blue error bars) for binomial vital rates. Simulated variation for fecundities however somewhat underestimated real variation in fecundities for some plant species, such as *Taxus floridana* (blue error bars; Fig. S3.1b).

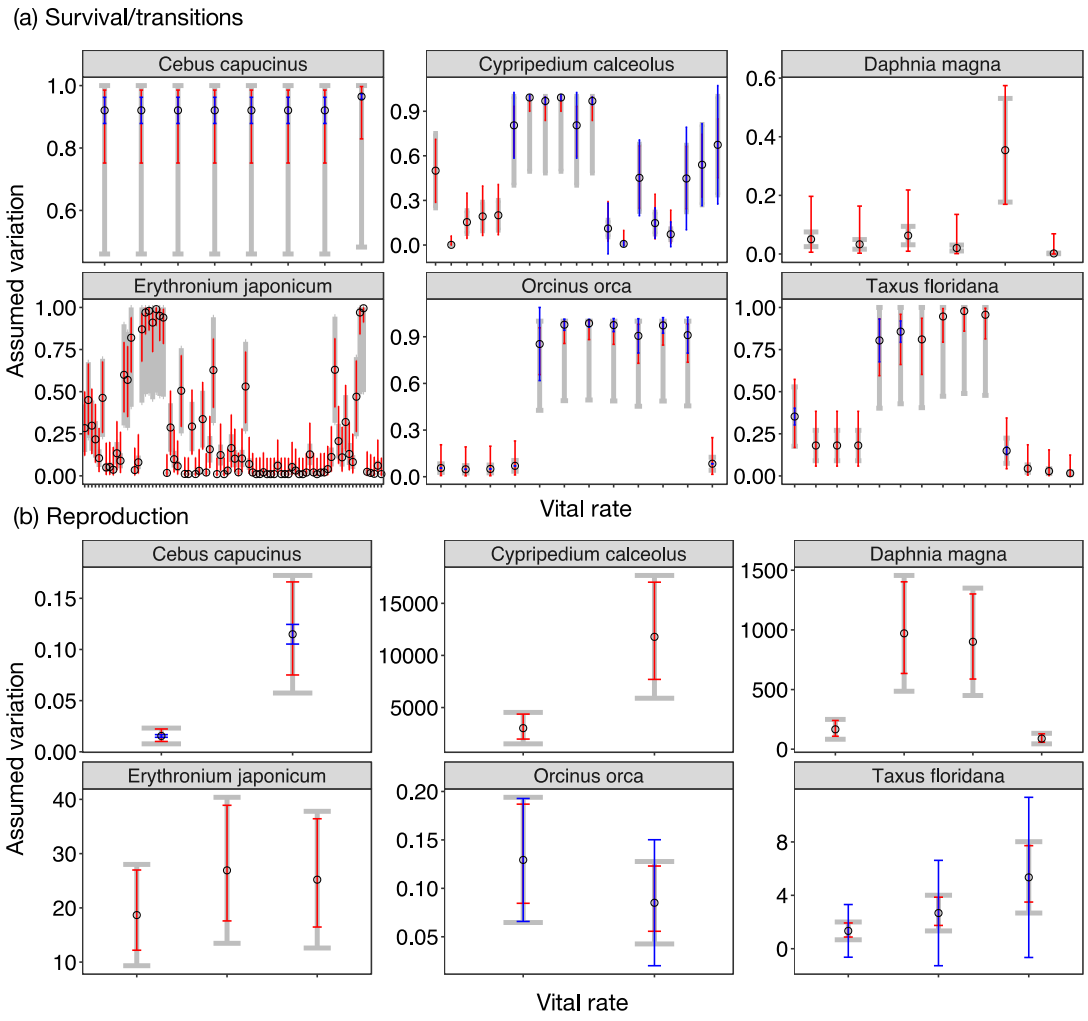

Figure S3.1 Simulated variation of average vital rates (points) among good (upper error bar) and bad (lower error bar) environments for a subset of species. Red error bars show vital-rate variation produced by assuming a gamma (for reproduction) and beta (for survival/transitions) distribution for vital rates and imposing a CV_{max}. Grey error bars show variation modeled under no a-priori assumption of vital-rate distribution. Blue bars show observed standard deviation (see Appendix S4) for a subset of species.

From the simulations of log λ_s at the three different temporal autocorrelation coefficients (v_1 = -0.3, 0, and 0.3) (Fig. S3.2), we obtained the sensitivity of log λ_s to v_1, S^{v_1}, as the absolute changes in log λ_s in response to the absolute changes in v_1.

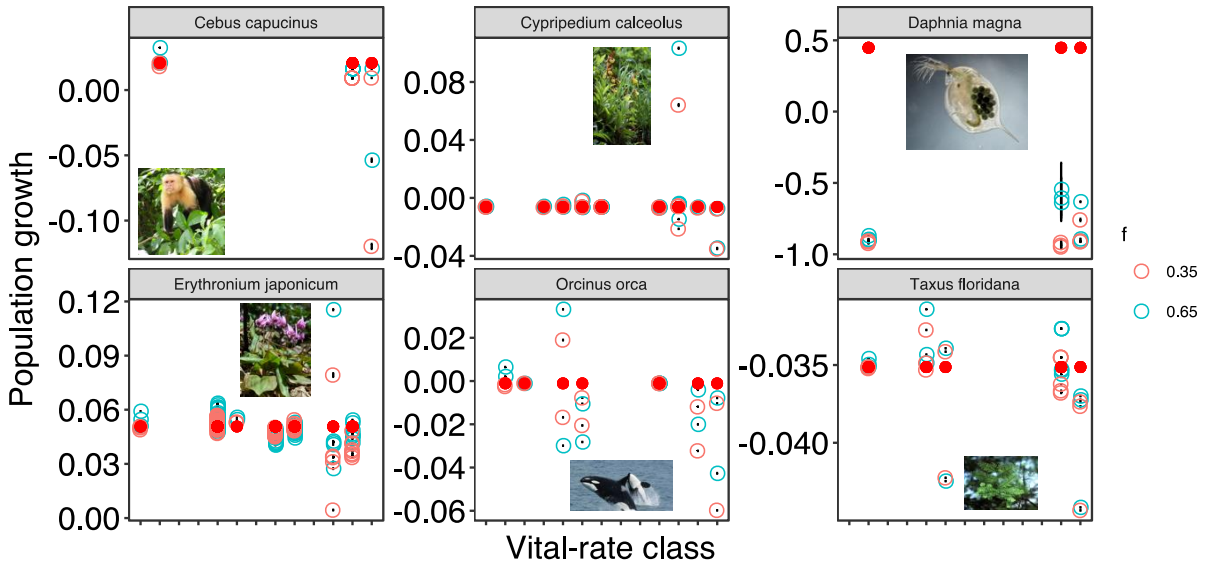

Figure S3.2 Distribution of the stochastic growth rate, log λ_s (open points) among simulations of population dynamics after perturbing vital rates using two different frequencies of the good environment (*f*; different point colors). Results for a subset of six species (at CV = 0.8 and v_1 = 0.3) are shown. See *lambdas_CV_0.8.pdf* and See *lambdas_CV_0.8_v1_0.3.pdf* for all species and v_1. Filled red points show deterministic λ of the average MPM. Error bars show 95 % C.I.

Repeating simulations with different ranges of v_1 did not significantly change S^{v_1}. We then modeled the relationship between S^{v_1}, the simulation parameters CV and *f* (long-term frequency of good environmental state), vital rates, and life-history strategies using generalized additive models (GAMs) to account for non-linearity of relationships. We used the R package *mgcv* to fit GAMs (Wood 2006). In parameterizing the GAMs, we used tensor product smooth terms (*te*), with thin-plate regression splines as the marginal bases for the effects of PCA 1 and PCA 2, and parametric terms penalized by a ridge penalty as bases for the random effect of population (`simLambdaTAC.R`). When applying smooths, we used four-knot locations for each predictor and applied and a degrees-of-freedom inflation factor (gamma) of 1.4 to avoid overly flexible smooths. We assumed a log-normal distribution of S^{v_1}. We first fitted log(S^{v_1}) as a function of

CV and *f*, assuming that phylogenetic dependencies similarly affected $\log(S^{v_1})$ at each CV and *f* level. We considered the following models, and the most parsimonious model as determined by AIC is highlighted in bold:

(1) $\log(S^{v_1})$ = *s*(MPMdimension) + *s*(population)

(2) $\log(S^{v_1})$ = CV + *s*(MPMdimension)+ *s*(population)

(3) $\log(S^{v_1})$ = CV + *f* + *s*(MPMdimension)+ *s*(population)

(4) $\log(S^{v_1})$ = CV × *f* + *s*(MPMdimension)+ *s*(population)

For **each combination of CV and *f***, we then modeled $\log(S^{v_1})$ as a function the two PCA axes describing different life histories (Appendix S2), vital-rate classes (see below), and the interaction of the three predictors:

(1) $\log(S^{v_1})$ = *s*(MPMdimension) + *s*(population)

(2) $\log(S^{v_1})$ = *s*(MPMdimension) + *s*(population) + *te*(PCA 1)

(3) $\log(S^{v_1})$ = *s*(MPMdimension) + *s*(population) + *te*(PCA 1) + *te*(PCA 2)

(4) $\log(S^{v_1})$ = *s*(MPMdimension) + *s*(population) + *te*(PCA 1, PCA 2)

(5) $\log(S^{v_1})$ = *s*(MPMdimension) + *s*(population) + *te*(PCA 1, PCA 2) + vital rate class

(6) $\log(S^{v_1})$ = *s*(MPMdimension) + *s*(population) + *te*(PCA 1, PCA 2) + vital rate class + *te*(PCA 1, by=vital rate class)

(7) $\log(S^{v_1})$= *s*(MPMdimension) + *s*(population) + *te*(PCA 1, PCA 2) + vital rate class + *te*(PCA 1, by=vital rate class) + *te*(PCA 1, by=vital rate class)

(8) **$\log(S^{v_1})$= *s*(MPMdimension) + *s*(population) + vital rate class + *te*(PCA 1, PCA 2, by=vital rate class)**

In addition, **for each CV and *f***, we tested for the significance of major habitat type in explaining variation in $\log(\overline{S^{v_1}})$:

(9) $\log(S^{v_1})$= *s*(MPMdimension) + *s*(population) + vital rate class + *te*(PCA 1, PCA 2, by=vital rate class) + habitat

(10) $\log(S^{v_1})$= *s*(MPMdimension) + *s*(population) + vital rate class + *te*(PCA 1, PCA 2, by=vital rate class) + habitat + *te*(PCA 1, by=habitat)

(11) $\log(S^{v_1})$= *s*(MPMdimension) + *s*(population) + vital rate class + *te*(PCA 1, PCA 2, by=vital rate class) + habitat + *te*(PCA 1, by=habitat) + *te*(PCA 2, by=habitat)

(12) $\log(S^{v_1})$= *s*(MPMdimension) + *s*(population) + vital rate class + *te*(PCA 1, PCA 2, by=vital rate class) + habitat + *te*(PCA 1, PCA 2, by=habitat)

(13) $\log(S^{v_1})$= *s*(MPMdimension) + vital rate class + *te*(PCA 1, PCA 2, by=vital rate class) + habitat + *te*(PCA 1, PCA 2, by=habitat)

Because the phylogenetically-informed PCA corrected for the phylogenetic non-independence among species (Appendix S2), we did not consider additional phylogenetic information in models including PCA scores. The predictions of the distribution of S^{v_1} across life histories, vital-rate classes, and major habitat types at CV = 0.5 and *f* = 0.65 are shown in Fig. 3 in the main text. Fig. S3.3 shows equivalent predictions for the remaining five combinations of CV and *f*, while Fig. S3.4 shows predictions obtained when omitting CV_{max} from simulations of vital-rate variation (at CV = 0.5 and *f* = 0.65).

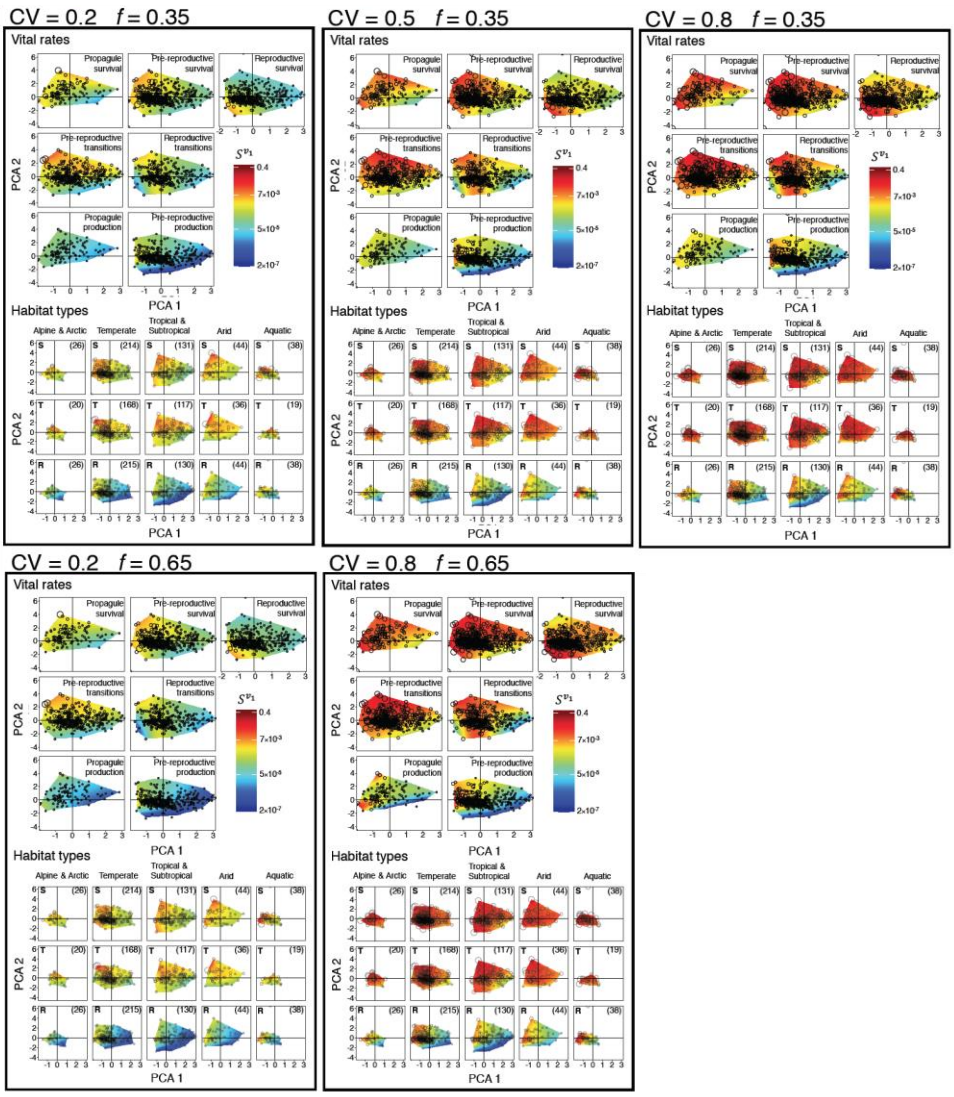

Figure S3.3 Fast life histories (along PCA 1) across reproductive strategies (along PCA 2) show highest sensitivities of the stochastic growth rate, log λ_s, to temporal autocorrelation (S^{ν_1}) across coefficients of variation (CV) and frequencies of good environmental states (f) used in simulations. Raster plots show predictions of S^{ν_1} across the two PCA axes after perturbing vital-rate classes and for five different habitat types. Predictions were limited to the range of observed PCA scores. Points show raw S^{ν_1} for the vital rates and habitat types obtained from simulations. Point sizes are proportional to S^{ν_1} values. Log values of predictions are plotted to facilitate visualization.

Omitting CV_{max} increased sensitivities of stochastic growth rates to autocorrelation for long-lived populations, in particular ones with increasingly iteroparous reproduction (Fig. S3.4). This occurs because without a CV_{max}, which constrains the variation on high average binomial

vital rates (Fig. S3.1), these latter vital rates were more variable (particularly downward; Fig. S3.1) and thus more sensitive to temporal autocorrelation.

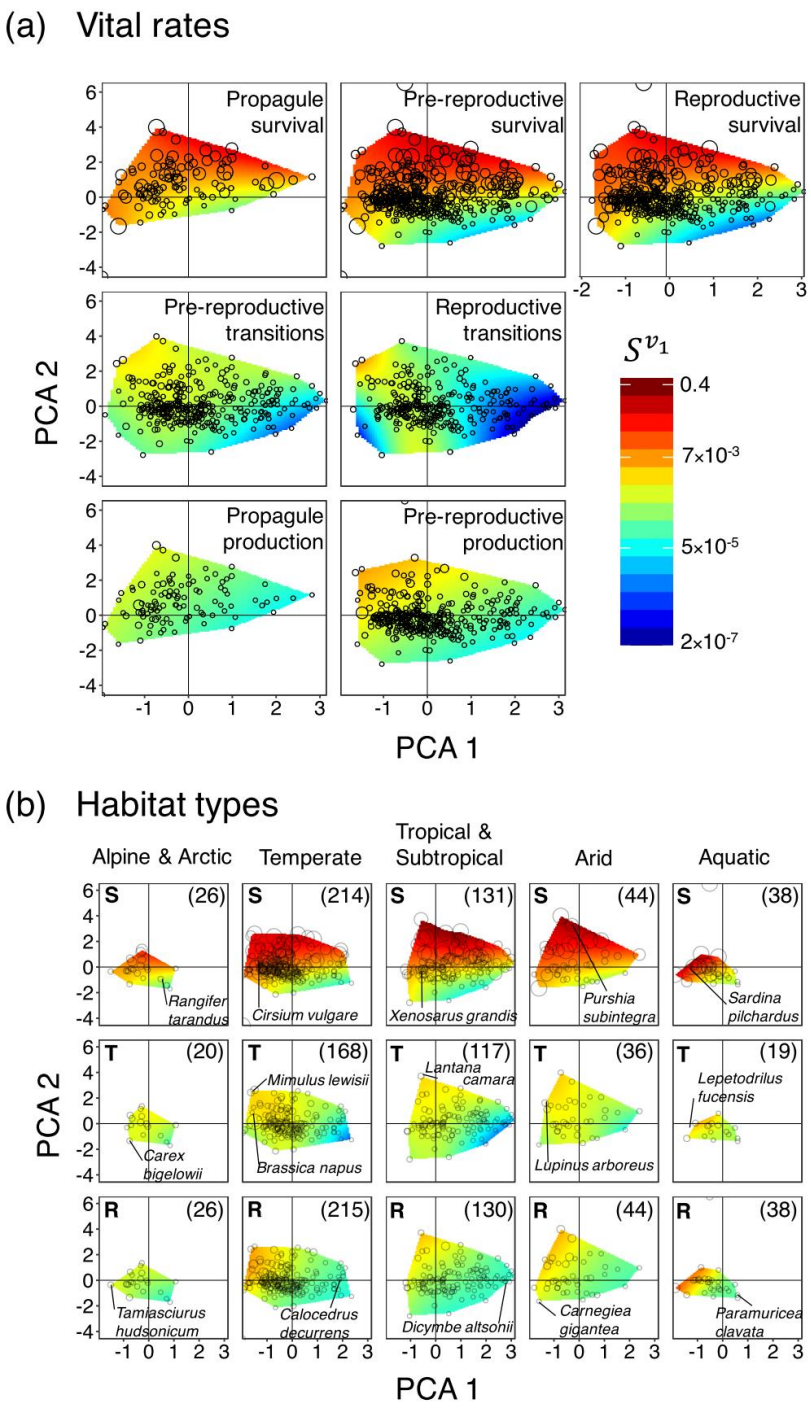

Figure S3.4 Fast life histories (along PCA 1) across reproductive strategies (along PCA 2) generally show highest sensitivities of the stochastic growth rate, log λ_s, to temporal autocorrelation (S^{v_1}). Raster plots show predictions of S^{v_1} across the two PCA axes after perturbing various classes of vital rates across all habitats (a) and for five different habitat types (b). In the simulations, a CV_{max} was not imposed on binomial vital rates. In (b), vital-rate

classes include survival (S), stage/age transitions (T), and reproduction (R). Predictions were limited to the range of observed PCA scores. Number of vital-rate samples in each habitat are shown in parentheses. Points are proportional to raw S^{v_1} for obtained from simulations. The results of vital-rate perturbations at CV = 0.5 and f = 0.65 are shown here.

However, even when a CV_{max} was not imposed, fast life histories remained more sensitive to changes in the patterning of environmental states than slow life histories (compare Fig. S3.4 with Fig. 3). In fact, S^{v_1} obtained from simulations in which CV_{max} were omitted (Fig. S3.4) were similar to S^{v_1} obtained under the highest CV simulated and including CV_{max} (Fig. S3.3).

As vital rates related to reproduction may show a CV > 1 (Fig. S3.1), we performed additional simulations of population dynamics altering reproduction between good and bad environmental states using CV = 1.5, 2.5, or 3.5 (keeping the remaining vital rates at their averages). These increased CV S^{v_1} overall but did not change the patterns of S^{v_1} variation among life-history strategies when perturbing reproduction (Fig. S3.5). S^{v_1} obtained from increased CV were highly correlated with ones obtained from CV = 0.5 (and 0.2 or 0.8; not shown), with Pearson's correlation coefficients of > 0.98 across comparisons (Fig. S3.5 a).

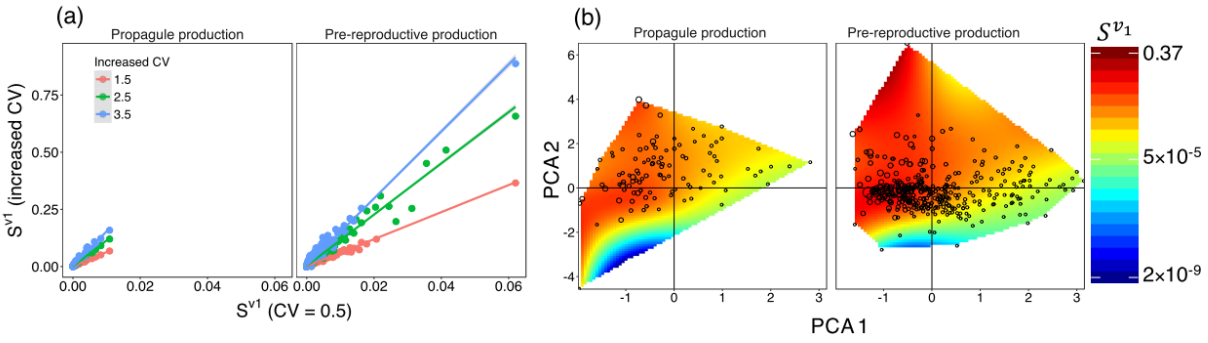

Figure S3.5 (a) Correlation between sensitivities of the stochastic growth rate, log λ_s, to temporal autocorrelation (S^{v_1}) using CV = 0.5 to perturb reproduction vital rates and S^{v_1} using higher CV (Pearson's correlation coefficients > 0.98 for all six comparisons); Lines show simple regression models fit to data. (b) Raster plots show predictions of S^{v_1} across the two PCA axes after perturbing various reproduction using a CV = 3.5. Predictions were limited to the range of observed PCA scores. Number of vital-rate samples in each reproduction class are shown in parentheses. Points are proportional to raw S^{v_1} for obtained from simulations. All results are shown at f = 0.65.

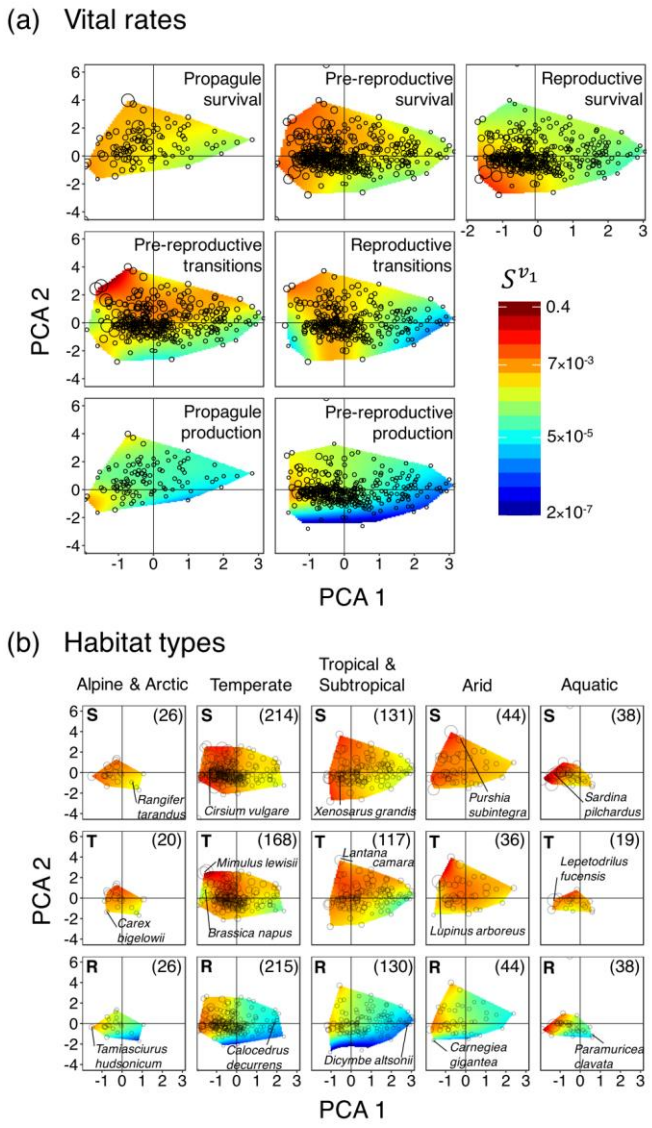

Figure S3.6 Raster plots show predictions of sensitivities of the stochastic growth rate, log λ_s, to temporal autocorrelation (S^{v_1}) across the two PCA axes after perturbing various classes of vital rates across all habitats (a) and for five different habitat types (b). When calculating S^{v_1}, change from 0 to negative autocorrelation (v_1 = -0.3) were considered (analyses in the main text showed results based om positive changes). In (b), vital-rate classes include survival (S), stage/age transitions (T), and reproduction (R). Predictions were limited to the range of observed PCA scores. Number of vital-rate samples in each habitat are shown in parentheses. Points are proportional to raw S^{v_1} for obtained from simulations. The results of vital-rate perturbations at CV = 0.5 and f = 0.65 are shown here.

S^{v_1} also remained similar regardless of whether temporal autocorrelation changed from 0 to 0.3 (making the occurrence of long temporal sequences of one give environmental state more likely) or from 0 to -0.3 (making annual changes between environments more likely; Fig. S3.6).

In all the models fitting S^{v_1} as a function of vital rates and life histories (Fig. S3.3a), we grouped vital rates into classes as described in Appendix S1. When we modeled S^{v_1} as a function habitat type (Fig. S3.3b), we grouped vital rates into three major classes (survival, transitions, and reproduction) in order to ensure adequate sample size of classes per habitat type (Fig. S3.3b). For each class, we summed S^{v_1} across individual vital rates. Using sums instead of averages was appropriate, as S^{v_1} for species that responded to temporal autocorrelation were proportional to relative elasticities of vital rates (calculated from the average MPM – for simplicity - as in Franco & Silvertown 2004; Fig. S3.7a) and therefore decreased with the total number of vital rates in an MPM (Fig. S3.7b). In addition, we accounted for MPM dimension in all models (see above).

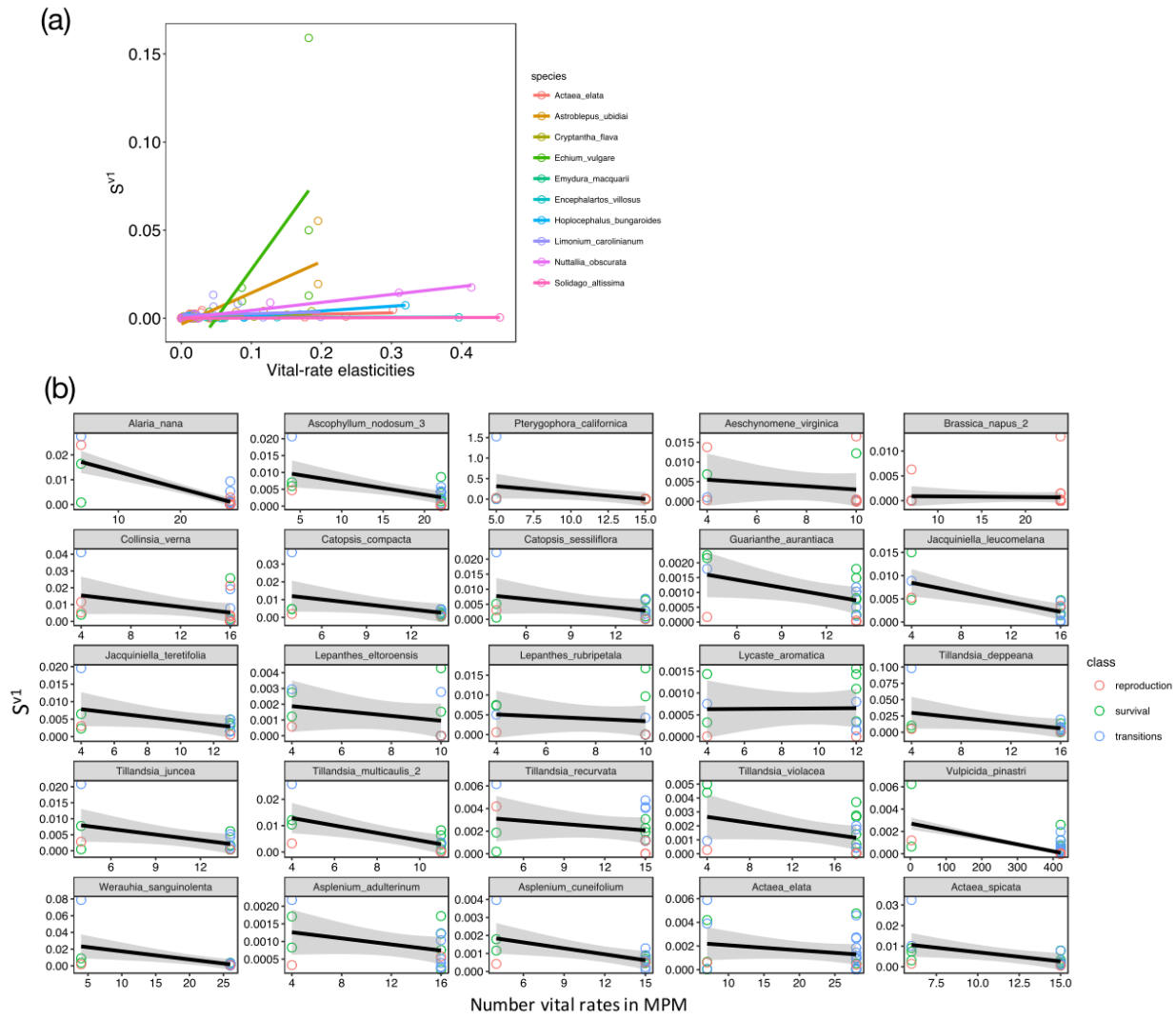

Figure S3.7 Sensitivities of the stochastic growth rate, log λ_s, to temporal autocorrelation (S^{v_1}) at each vital rate are positively correlated with relative elasticities of deterministic λ to vital-rate changes (a) and are negatively correlated with dimension of MPMs (see below for collapsing). Lines show simple regression models fit to data (± prediction error in b). Results for a subset of populations modeled are shown. For all populations, see *MatDim.pdf*.

However, the relationships presented in Fig. S3.7 were not perfectly linear, and the dimension of MPMs did explain a significant proportion of S^{v_1}variance in some GAMs (see above), To test how much MPM dimension affected S^{v_1} patterns, we collapsed the dimensions of each MPM to a four-stage structure represented by 12 vital rates (Fig. S3.8) following Salguero-Gómez & Plotkin (2011). The 12 vital rates describe four processes: stage-specific survival (σ), progression (γ), retrogression (ρ), and reproduction (φ).

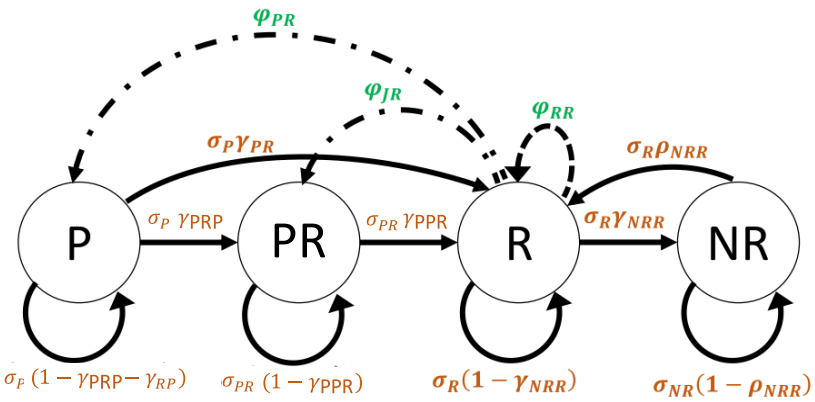

Figure S3.8 A standardize life cycle that can represent any of the species' populations used in this study, after stages were collapsed to a four-stage structure with stages: propagule (P), juvenile (J), reproductive (R), and non-reproductive (NR). Species' populations may differ in the values for the 12 vital rates [stage-specific survival (σ), progression (γ), retrogression (ρ), and fecundity (φ)].

We then repeated all simulations detailed above on the collapsed vital rates. Fig. S3.9 shows that S^{v_1}patterns across life histories (PCA axes) using collapsed vital rates did not differ substantially from results based on original vital rates, indicating that MPM dimension, while affecting the overall magnitude of S^{v_1}, does not affect life-history differences in S^{v_1} patterns.

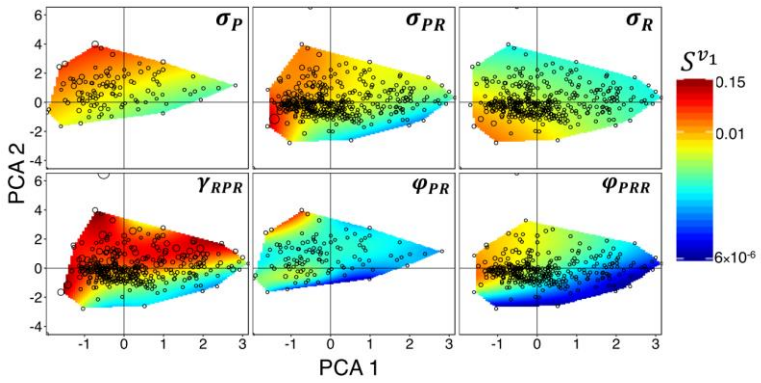

Figure S3.9 Fast life histories (along PCA 1) across reproductive strategies (along PCA 2) show highest sensitivities of the stochastic growth rate, log λ_s, to temporal autocorrelation (S^{v_1}) when simulating collapsed vital rates. Raster plots show predictions of S^{v_1} across the two PCA axes after perturbing individual vital rates propagule survival (σ_P), pre-reproductive survival (σ_{PR}), reproductive survival (σ_R), progression from pre-reproductive to reproductive (γ_{RPR}), propagule production (φ_{PR}), and pre-reproductive production (φ_{PRR}). Points show raw S^{v_1} for the vital rates. The results of vital-rate perturbations at CV = 0.5 and f = 0.65 are shown here.

Appendix S4 Empirical analyses

For a subset of 109 populations, 3 or more annual MPMs were provided in COMADRE and COMPADRE. We used these studies to calculate vital-rate variances and correlations among vital rates as shown in `getVitalRates_CoVariance.R`. That is, we obtained within-year correlations among vital rates from each study site per species and then calculated the average correlations across sties. We then generated random values for each vital rate per MPM from a multivariate distribution of correlated vital rates given their means obtained from the average MPMs (`simLambdaTAC_varCov.R`). We generated such multivariate distributions using copulas following Koons *et al*. (2008). Copulas combine different univariate marginal distributions, here gamma for reproduction and beta for survival and transitions, into a multivariate distribution based on a specified vital-rate correlation structure (see Yan 2007). We then generated 1,000 MPMs from the multivariate distribution of vital rates (`simLambdaTAC_varCov.R`) and simulated stochastic population dynamics as described in Appendix S3 (with the exception that no CV had to be modeled). During the simulations, an MPM was assigned to the good or bad environmental state if its deterministic growth rate, λ, was above or below, respectively, λ obtained from the average vital-rate MPM (as given in COMADRE/COMPADRE). To test whether sensitivity of the stochastic population growth rate (log λ_s) to temporal autocorrelation (S^{v_1}) differed between life histories and habitats, GAMs analogous to the ones shown in Appendix S3 were used.

S^{v_1} obtained from simulations based on empirically observed CV were highly correlated, on a log scale, with S^{v_1} obtained from simulated CV (Pearson's correlation coefficient = 0.58, p <0.001).

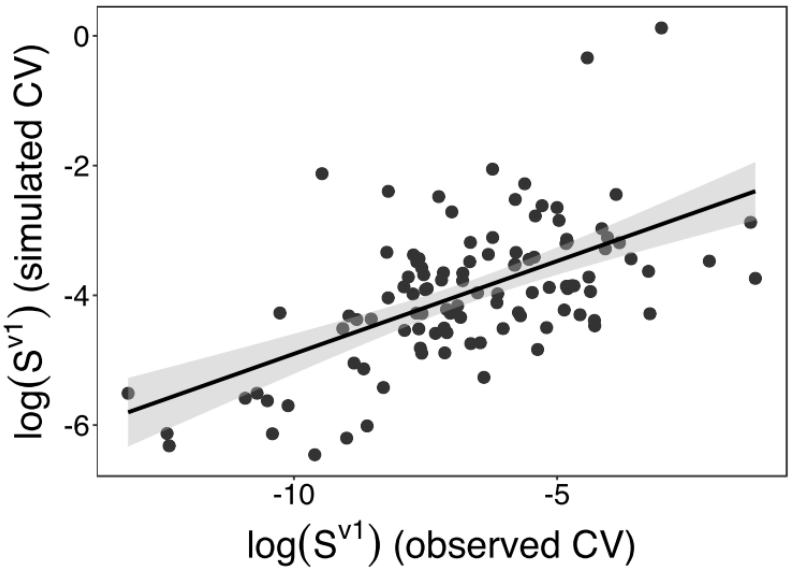

Figure S4.1 Correlation between sensitivities of the stochastic growth rate, log λ_s, to temporal autocorrelation (S^{v_1}) when observed CV vs. simulated CV was used in simulations of stochastic population dynamics. For the simulated CV, S^{v_1} are summed across all vital rates and results for CV = 0.5 are shown (the strength of the correlation did not change when CV = 0.2 or 0.8 was used). The line represents a simple regression model fit to the data.

In addition to validating our simulations with analyses using observed vital-rate variation, we interested in the analyses of temporal autocorrelation in the empirical studies from with the MPMs used in our study were obtained. We therefore searched Web of Science (http://www.webofknowledge.com) for each study population using the following search criteria: TS = Latin name of study species AND TS = (temporal autocorrelation OR Markov chain* OR stochastic model* OR serial correlation OR first-order autocorrelation* OR auto regressive*). For each resulting species' publication, we noted whether autocorrelated environmental variation was explicitly examined, and whether it significantly affected stochastic population dynamics. (see the script `figure 4 main text.R`). Overall, out of the 454 populations used in this study, previous studies considered stochastic changes in environmental states when assessing population dynamics in 38% of the cases (171 publications). Of these, 36 (or 21 %) directly (e.g.,

through autoregressive models) or indirectly (e.g., through Markov chain transitions of environmental states) considered autocorrelated environmental variation to have a significant effect on population dynamics. Out of these 36 study populations in turn, 70 % showed relatively high S^{v_1} in our simulations (> the 50th percentile across *f* and CV); and 86 % showed S^{v_1} the 25th percentile. However, 44 % of the populations that were not previously assessed under consideration of temporal patterning in environmental states also had relatively high S^{v_1} (> 50th percentile).

References

Caswell, H. (2001). *Matrix Population Models: Construction, Analysis and Interpretation.* 2nd ed. Sinauer Associates, Sunderland, US, pp. 722.

Chamberlain, S. & Szocs, E. (2013). taxize - taxonomic search and retrieval in R. *F1000Research,* **2**, 191.

Cohen, A.A. (2004). Female post-reproductive lifespan: a general mammalian trait. *Biol. Rev.*, **79**, 733-750.

Franco, M. & Silvertown, J. (2004). A comparative demography of plants based upon elasticities of vital rates. *Ecology*, **85**, 531-538.

Hinchliff, C.E., Smith, S.A., Allman, J.F., Burleigh, J.G., Chaudhary, R., Coghill, L.M., *et al.* (2015). Synthesis of phylogeny and taxonomy into a comprehensive tree of life. *Proc. Natl. Acad. Sci.* **112,** 201423041.

Keyfitz, N. (1977). *Applied Mathematical Demography*. Springer, New York, US.

Koons, D.N., Metcalf, C.J. & Tuljapurkar, S. (2008). Evolution of delayed reproduction in uncertain environments: a life-history perspective. *Am. Nat.,* **172,** 797-805.

Legendre, P. & Legendre, L. (2012). *Numerical Ecology*, 3rd ed. Elsevier, London, pp. 1006.

Michonneau, F., Brown, J. & Winter D. (2016). rotl, an R package to interact with the Open Tree of Life data. *PeerJ Preprints*, **4**, e1471v3.

Orme, D., Freckleton, R., Thomas, G., Petzoldt, T., Fritz, S., *et al.* (2013). *Caper: comparative analyses of phylogenetics and evolution in R*. Vienna (Austria): Comprehensive R Archive Network [Cited 2014 Nov 21]. Available from: http://CRAN.R-project.org/package=caper.

Paradis, E., Claude, J. & Strimmer, K. (2004). APE: Analyses of phylogenetics and evolution in R language. *Bioinformatics*, **20,** 289–290.

Revell, L. J. (2009). Size-correction and principal components for interspecific comparative studies. *Evolution*, **63**, 3258-3268.

Revell, L.J. (2012). phytools: An R package for phylogenetic comparative biology (and other things). *Methods Ecol. Evol.*, **3,** 217–223.

Salguero-Gómez, R., Jones, O.R., Archer, C.R., Buckley, Y.M., Che-Castaldo, J., Caswell, H., *et al.* (2015). The COMPADRE Plant Matrix Database: an open online repository for plant demography. *J. Ecol.*, **103**, 202-18.

Salguero-Gómez, R., Jones, O.R., Archer, C.R., Bein, C., Buhr, H., Farack, C., *et al.* (2016a). COMADRE: a global data base of animal demography. *J. Anim. Ecol.*, **85**, 371-384.

Salguero-Gómez, R., Jones, O.R., Jongejans, E., Blomberg, S.P., Hodgson, D.J., Mbeau-Ache, C., *et al*. (2016b). Fast–slow continuum and reproductive strategies structure plant life-history variation worldwide. *Proc. Natl. Acad. Sci.*, **113**, 230-235.

Salguero-Gómez, R. & Plotkin, J.B. (2010). Matrix dimensions bias demographic inferences: implications for comparative plant demography. *Am. Nat.*, **176**, 710-722.

Wood, S.N. (2006). *Generalized Additive Models: An Introduction with R*. Chapman and Hall/CRC, London, pp. 416.

Yan, J. (2007). Enjoy the joy of copulas: with a package copula. *J. Stat. Softw.*, **21**, 1-21.